Available online at www.sciencedirect.com
SCIENCE DIRECT
Journal of Molecular Catalysis A: Chemical 244 (2006) 33–40
JOURNAL OF MOLECULAR CATALYSIS A: CHEMICAL
www.elsevier.com/locate/molcata

Studies on MCM-48 supported cobalt catalyst for Fischer–Tropsch synthesis

Hualan Li [a], Shuguo Wang [a], Fengxiang Ling [b], Jinlin Li [a,*]

[a] *Hubei Key Laboratory for Catalysis and Material Science, College of Chemistry and Material Science, South-Central University for Nationalities, Wuhan 430074, China*
[b] *Fushun Research Institute of Petroleum and Petrochemicals, Fushun 113001, China*

Received 4 July 2005; received in revised form 30 August 2005; accepted 30 August 2005
Available online 4 October 2005

Abstract

MCM-48 molecule sieve was used as a support of cobalt catalyst for Fischer–Tropsch synthesis (FTS). Co/MCM-48 catalysts were prepared using incipient witness impregnation method with cobalt loadings of 5, 10 and 15 wt.%, respectively. The catalysts were characterized by N_2 physisorption, X-ray diffraction (XRD), temperature programmed reduction (TPR), hydrogen temperature programmed desorption (H_2-TPD) followed by pulse oxygen titration and transmission electron microscopy (TEM). The catalytic properties for FTS were tested in a fixed bed reactor. TPR and oxygen titration indicated different extent of overall reduction of Co cobalt species in different cobalt content catalysts. With increasing Co loading, CO conversion and C5+ selectivity first increased remarkably and then remained nearly invariable. Lower reducibility of smaller cobalt particles on 5Co/MCM-48 is likely to be one of the reasons responsible for the lower CO conversion and highest methane selectivity. Co loading exceeding 10 wt.% had no significant effect on FTS properties of the catalysts.

Keywords: Fischer–Tropsch synthesis; MCM-48; Cobalt; Catalyst; Mesoporous silica

1. Introduction

Fischer–Tropsch (FT) synthesis is a process for hydrocarbon production from carbon monoxide and hydrogen. The synthetic fuels produced via FT synthesis have high cetane numbers, low contents of sulfur and aromatics. This makes them suitable for diesel engines and friendly for environment [1]. Supported Co-based catalysts have been widely used to achieve high yields of paraffinic hydrocarbons in FT synthesis [2–6]. Cobalt is usually supported on a high surface area support such as SiO_2 [7–9], Al_2O_3 [7], zeolites [10] and TiO_2 [7] with microporous and mesoporous structures in order to obtain a high metal dispersion. These conventional mesoporous supports are irregularly spaced and their pore sizes are broadly distributed. Thus, it is rather hard to study the effect of support and its porosity on FT reaction rate and hydrocarbon selectivity [11]. Highly ordered mesoporous silica, such as MCM-41 [12], FSM-16 [13], SBA-15 [14] and HMS [15], have been recently used as a support for metal catalysts, which were found to have well-defined periodic mesopores, consequently provide very narrow pore size distributions, and possess large pore volumes of 1–2 cm^3/g and high surface areas reaching 1000 m^2/g. The pore diameters can be controlled in the range of 2–30 nm by using various surfactants, additives, and different synthetic conditions [16]. The narrow pore size distributions are suitable for evaluation of pore size and texture effects on cobalt dispersion and also it may make it possible to design new catalysts with higher productivity for long chain hydrocarbons. Thus, the use of periodic mesoporous silicas as supports for preparing Co-based FTS catalysts has been recently explored [17–22].

Catalytic behavior of silica supported cobalt catalysts in FT synthesis was found to depend on the nature of cobalt species, cobalt particle size and catalyst mesoporous structure. The properties of the cobalt particles were greatly affected by the pore size of the mesoporous support. Previous reports showed that reducibility of cobalt particles supported by silica [20,23,24], titania [25] and alumina [26] depended mostly on their sizes. Smaller cobalt particles are usually more difficult to reduce than larger ones. For example, with alumina supported cobalt catalysts, even though the true metal cluster size is smaller at

* Corresponding author. Tel.: +86 27 67843016; fax: +86 27 67842752.
E-mail address: lij@scuec.edu.cn (J. Li).

1381-1169/$ – see front matter © 2005 Elsevier B.V. All rights reserved.
doi:10.1016/j.molcata.2005.08.050

lower loadings, the poor extent of reduction leads to a low cobalt surface metal active site density under FT conditions. Heavier loadings are often used to increase the cluster size and thereby break the cobalt oxide–support interaction, resulting in increased extent of reduction and leading to improved cobalt surface active site densities. It is often considered [7,15] that the presence of larger cobalt particles leads to higher selectivity to heavier hydrocarbons.

Considering the discussion above, larger cobalt particles sizes formed in wider pore mesoporous supports, such as SBA-15, and were more reducible leading to catalysts with higher catalytic activity and lower methane selectivity than smaller particles in narrower pore materials, such as MCM-41. Lower FT activity and higher methane selectivity observed on the narrow pore cobalt catalysts are principally attributed to the lower reducibility of small cobalt particles [18,20].

It is usually suggested that the size of supported metal and oxide particles and thus their catalytic behavior are principally affected by overall metal content in supported catalysts. It is generally assumed that an increase in metal loading would almost automatically result in lowering of metal dispersion [27]. Co/SBA-15 catalysts cobalt loadings of 10–40 wt.% were prepared and a maximum CO conversion was obtained for the catalyst loaded with ca. 30 wt.% Co presenting the highest density of surface Co^0 sites. This finding highlights the importance of further considering the impact of the cluster size on the reducibility of cobalt clusters. That is, at low cobalt loadings, the cobalt oxide–support interaction is strengthened, making it difficult to achieve reduction of the cobalt clusters and therefore, generate surface active sites. Product selectivities were also influenced by Co loading. The product distribution shifted toward the formation of lighter hydrocarbons (methane, C2–C4) for the less reducible low-loaded sample [28].

The synthesis of the silica-based M41S was first reported in 1992 [29]. The specific properties of these materials are large surface areas and a narrow pore-size distribution. MCM-48, as a member of M41S, has a cubic structure indexed in the space group *Ia*3*d* [30], recently modelled as a gyroid minimal surface with its high specific surface area up to 1600 $cm^2\,g^{-1}$ specific pore volume up to 1.2 $cm^3\,g^{-1}$ and high thermal stability. This is because of its interwoven and branched pore structure, which provides more favourable mass transfer kinetics in catalytic and separation applications than MCM-41 with its unidirectional pore system [31]. Various ordered mesoporous silica for cobalt catalysts have been used, but an application of MCM-48 as metal support to cobalt-based FT catalysts has not previously been reported. In this work, MCM-48 was utilized to investigate how MCM-48, its pore size and Co loading affect surface reaction parameters during CO hydrogenation. Co/MCM-48 catalysts with different Co content were prepared, characterized by N_2 physisorption, X-ray diffraction (XRD), transmission electron microscopy (TEM), temperature programmed reduction (TPR), hydrogen temperature programmed desorption (H_2-TPD) with pulse oxygen titration, and tested in a fixed-bed reactor for the Fischer–Tropsch synthesis reaction.

2. Experimental

2.1. Synthesis of MCM-48 and catalyst

MCM-48 was synthesized by the conventional hydrothermal pathway similar to the procedure described by Wang et al. [32]. *n*-Hexadecyltrimethylammonium bromide ($C_{16}H_{33}(CH_3)_3$–NBr, template) was dissolved in deionized water, sodium hydroxide and tetraethoxysilane (TEOS) were added. The molar composition of TEOS:NaOH:$C_{16}H_{33}(CH_3)_3$–NBr:H_2O was 1:0.48:0.4:55. The solution was stirred for about 30 min, charged into a polypropylene bottle and then heated at 383 K for 3 days. The sample was filtered, washed with water, and calcined at 823 K for 6 h to remove template. The calcined MCM-48 was used as a support for Co catalyst.

Co was introduced to the supports by incipient wetness impregnation using aqueous solutions of cobalt nitrate. After impregnation the catalysts were dried at 373 K and then calcined in a flow of air at 773 K for 5 h. The three catalysts were prepared with 5, 10 and 15 wt.% cobalt loading and denoted as 5Co/M, 10Co/M and 15Co/M, respectively.

2.2. Characterization techniques

2.2.1. BET measurements

Pore size distribution, BET surface area and pore volume were measured by Micromeritics ASAP2405 automatic system using nitrogen physisorption at 77 K. The specific surface area was estimated by the BET method. The pore size distribution and pore volume was determined by the BJH method [33].

2.2.2. XRD

X-ray diffraction patterns were obtained at room temperature in a Phillips X'pert diffractometer using monochromatized Cu Kα radiation. The scan range was 1–80° with 0.002° steps. The average particle sizes of Co_3O_4 were estimated from the Scherrer equation [34] using the most intense reflexion at $2\theta = 36.9°$

$$d = \frac{k\lambda}{B\cos\theta}\frac{180°}{\pi}$$

where d is the mean crystallite diameter, k (0.89) the Scherrer constant, λ the X-ray wave length (1.54056 Å) and B is the full width half maximum (FWHM) of Co_3O_4 diffraction peak.

The Co_3O_4 particle sizes in the calcined samples were then converted to the corresponding cobalt metal diameters in reduced catalysts by considering the relative molar volumes of Co^0 and Co_3O_4 using the equation: $d(Co^0) = 0.75 \times d(Co_3O_4)$. Then, the Co^0 metal dispersions can be calculated from the mean Co^0 particle sizes assuming a spherical geometry of the metal particles with uniform site density of 14.6 atoms/nm^2 as described in ref. [35] using $D = 96/d(Co^0)$, where D is the percentage dispersion and $d(Co^0)$ is the mean particle size of Co^0 in nm.

2.2.3. Temperature programmed reduction

The reduction behavior and the interaction between active phase and support of each catalyst were examined by using

temperature programmed reduction technique. The TPR experiments were carried out with a Zeton Altamira AMI-200 unit. The catalyst (ca. 0.12 g) was placed in a quartz tubular reactor, fitted with a thermocouple for continuous temperature measurement. The reactor was heated with a furnace designed and built to stabilize the temperature gradient and minimize the temperature error. Prior to the hydrogen temperature programmed reduction measurement, the calcined catalysts were flushed with high purity argon at 423 K for 1 h, and cooled down to 323 K. Then 10% H_2/Ar was switched on and the temperature was raised at a rate of 10 K min^{-1} from 323 to 1023 K (hold 30 min). The gas flow rate through the reactor was controlled by three Brooks mass flow controllers and was 30 cm^3 min^{-1}. The H_2 consumption (TCD signal) was recorded automatically by a PC.

2.2.4. Hydrogen temperature programmed desorption and O_2 titration

Hydrogen temperature programmed desorption was also carried out in a U-tube quartz reactor with the Zeton Altamira AMI-200 unit. The sample weight was about 0.2 g. The catalyst was reduced at 723 K for 12 h using a flow of high purity hydrogen and then cooled to 373 K under hydrogen flow. The sample was held at 373 K for 1 h under flowing argon to remove weakly bound physisorbed species prior to increasing the temperature slowly to 723 K. Then, the catalyst was held under flowing argon to desorb the remaining chemisorbed hydrogen and the TCD began to record the signal till the signal returned to the baseline. The TPD spectrum was integrated and the amount of desorbed hydrogen was determined by comparing to the mean areas of calibrated hydrogen pulses.

O_2 titration was also performed with the Zeton Altamira AMI-200 unit. After reduction under the conditions (as described above for H_2-TPD), the catalyst was kept in flowing Ar at 723 K and the sample was reoxidized by injecting pulses of high purity oxygen in argon. The extent of reduction was calculated by assuming metal Co was converted to Co_3O_4. The results were shown in Table 2.

2.2.5. Transmission electron microscopy

Transmission electron microscopy characterization of the samples was carried out by using a FEI Tecnai G^2 instrument. The samples were crushed in an agate mortar, dispersed in ethanol and dropped on copper grids. The Co_3O_4 average particle diameter and particle-size distribution were obtained by TEM. Between 100 and 300 particles coming from at least four different blind-coded images were measured. Unfocused or superimposed particles were discarded. From these data, the statistical average was calculated. Thus, only a rough indication on the size of the cobalt clusters can be given, due to the limited number of TEM images.

2.2.6. FT activity and selectivity

Fischer–Tropsch synthesis was performed in a fixed bed reactor (i.d. 2 cm) at 10 bar. The catalyst (ca. 6.0 g) was mixed with ca. 36.0 g carborundum and reduced in situ at atmosphere pressure. The reactor temperature was increased from ambient temperature to 373 K (hold 60 min) in a H_2 flow of 6 S L g^{-1} h^{-1}, then, increased to 723 K in 2 h and held for 12 h. Subsequently, the reactor was cooled down to 453 K. The syngas (H_2:CO = 2) was introduced to the reactor and the pressure was increased to 10 bar. The reactor temperature was increased to 503 K in 4 h and the reaction was carried out at 503 K. The products were collected in a hot trap and a cold trap in sequence. The effluent product gas was passed through an Agilent 3000GC for online analysis. The liquid product analysis was performed with an Agilent 6890GC equipped with a FID detector. The solid wax was analyzed with an Agilent 4890GC. The carbon monoxide conversion (X_{CO}%) was measured at the steady state and X_{CO}%, hydrocarbon selectivity have been averaged over the period of constant operation. The ratio of olefin/paraffin was calculated from the respective chromatogram peak areas.

3. Results and discussion

3.1. N_2 physisorption

The N_2 physisorption isotherms for the 10Co/M sample are shown in Fig. 1. BET surface areas, pore volumes and average pore diameters of the catalysts are given in Table 1. The isotherm of the catalyst presents a sharp inflection at a relative pressure of about 0.25, indicating a narrow distribution of pores in the mesopore range characteristic for this material. N_2 physisorption isotherms of the supported Co samples were similar to that of the original MCM-48, suggesting that the mesoporous structure of MCM-48 was mostly retained upon cobalt impregnation.

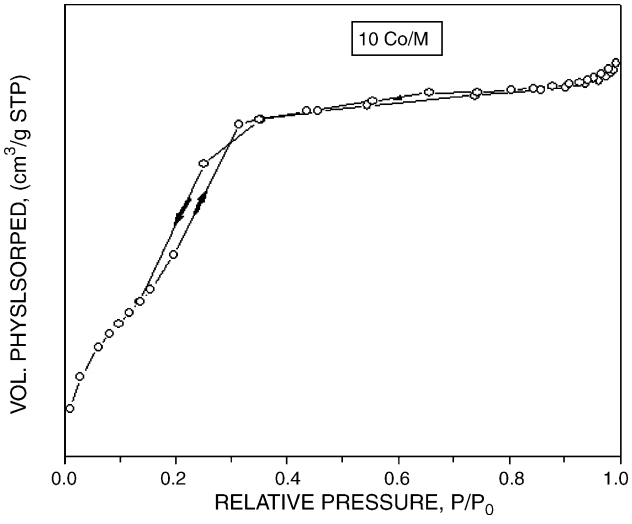

Fig. 1. Nitrogen physisorption isotherms of 10Co/M.

Table 1
N_2 physisorption results

Sample	BET surface area (m^2/g)	Pore volume (cm^3/g)	Average pore diameter (nm)
MCM-48	1127	1.1	2.6
5Co/M	776	0.72	2.4
10Co/M	734	0.68	2.3
15Co/M	626	0.58	2.4

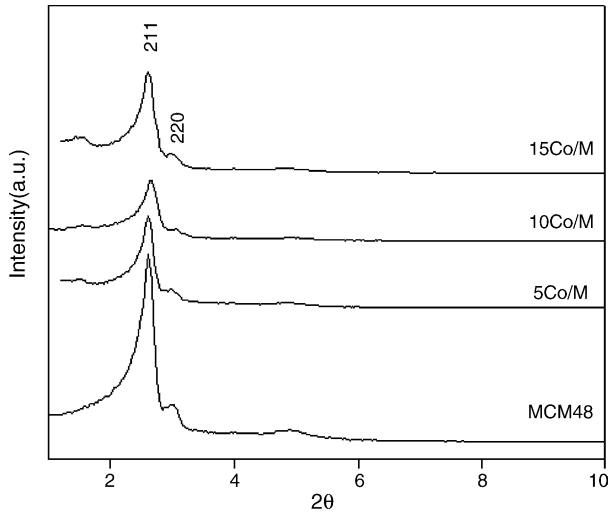

Fig. 2. XRD profiles for MCM-48 and catalysts.

The BET surface area and pore volumes of the catalysts decreased with increasing Co loading, the decrease however being more significant in the case of higher at larger Co loading catalysts. This may be caused by a partial blockage of the MCM-48 pores by cobalt oxide clusters and/or a partial collapse of the mesoporous structure.

3.2. X-ray diffraction

The XRD patterns at lower and higher diffraction angles of the calcined samples are displayed in Figs. 2 and 3, where those for MCM-48 support is also illustrated for comparison. The average crystallite sizes of Co_3O_4 and cobalt metal (Co^0) dispersion were calculated and listed in Table 2.

The MCM-48 provided distinct two diffraction lines due to SiO_2 (2 1 1), (2 2 0) planes (Fig. 2), showing cubic structures, as reported early [12,32]. When Co loading in the Co/MCM-48 was increased, the XRD profiles were almost unchanged and exhibited the highly diffraction peaks at low 2θ angles reflecting the ordered structure of MCM-48. It is evident that the cubic

Table 2
Characterization results of Co catalyst

Catalyst	Co_3O_4 crystallite diameter (nm)		Co^0 dispersion (%)		Extent of overall reduction (%)
	XRD	TEM	XRD	TPD and O_2 titration	O_2 titration
5Co/M	5	3	25.6	59.2	1.0
10Co/M	11	4.5	11.6	21.4	20.4
15Co/M	14	6.5	9.1	14.2	21.3

structures of the calcined MCM-48 are still retained to some extent even by adding 5–15 wt.% Co. But it was found that after loading Co, the intensity of the (2 1 1) MCM-48 reflection peak gradually decreased and the peak became broader. It suggested that the order of the MCM-48 may have partially collapsed during calcination and Co loading.

The diffraction peaks at 2θ of 31.3°, 36.9°, 45.1°, 59.4° and 65.4° (Fig. 3) indicate that after calcinations at 500 °C cobalt was primarily in the form of Co_3O_4 spinel on all the catalysts and Co species are highly dispersed. The higher the cobalt content is, the stronger the XRD intensity of Co_3O_4 is and the narrower the full width half maximum of Co_3O_4 diffraction peak is. It suggests that crystallite size increases and many larger particles formed at higher Co loading. The average sizes of Co_3O_4 crystallites detected were larger than the corresponding pore diameters, indicating that some of Co_3O_4 clusters are held outside the pores. It is probable that the Co particles present outside the pores can readily agglomerate to be crystallized due to weak interactions with surface SiOH groups of the support compared with those inside the pores [36]. Then when cobalt loading increased the cobalt particles outside the pore became larger because of agglomeration.

3.3. Temperature programmed reduction

The TPR profiles for the Co/MCM-48 catalysts are shown in Fig. 4. There are four H_2 consumption peaks in every profile,

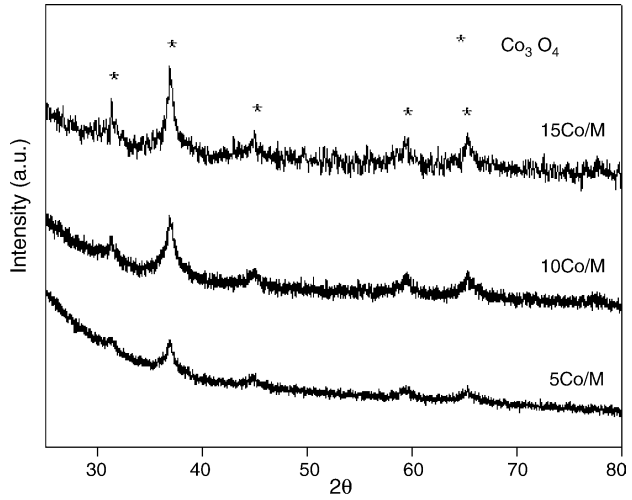

Fig. 3. XRD profiles for the catalysts.

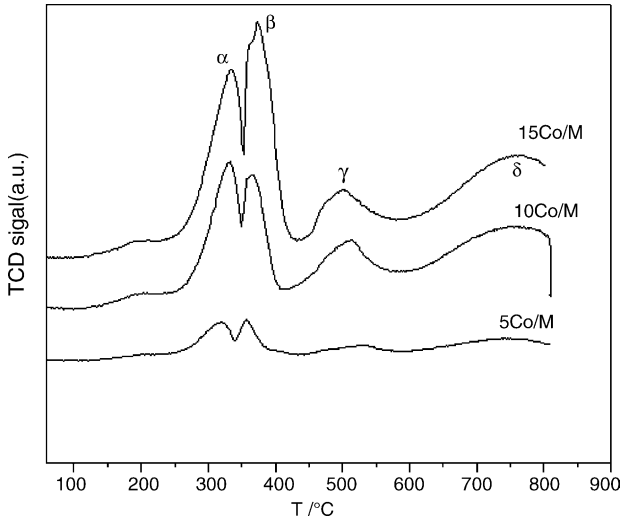

Fig. 4. TPR profiles for Co/MCM-48 catalysts.

with temperature ranges of about 220–360, 360–450, 500–600 and above 640 °C, respectively. The α peak could be assigned to the reduction of Co_3O_4 to CoO, and the β one to the subsequent reduction of CoO to Co^0 [37,38]. The relative intensity of the second reduction peak increased with Co loading, suggesting a higher reduction degree of CoO to metallic Co with increasing the mean diameter of Co_3O_4 particles. The reducibility of TPR 220–450 °C is directly related to the amount of active of Co^0 sites available for catalyzing FTS after standard reduction. The γ and δ peaks suggest the presence of surface Co species with different degrees of interaction with the support [28]. The γ peak indicates so a low strength of interaction between Co species and support which could not form the cobalt silicate species. The δ peak with the temperature range of 640–800 °C might be assigned to the reduction of cobalt silicate species formed during the catalysts preparing process.

The extent of Co reduction and Co^0 dispersion estimated from TPD and O_2 titration is given in Table 2. The extent of reduction of catalysts first increased rapidly and then slightly increased with increasing Co loading. It attributed to the size of Co_3O_4 on the catalysts, which larger cobalt oxide particles being much easily reduced.

3.4. Transmission electron microscopy

Micrographs of 5Co/M, 10Co/M and 15Co/M are shown in Figs. 5–7, respectively. TEM investigation provides the direct observation of the morphology and distribution of Co particles in the MCM-48. Images (Figs. 4–6) show the highly ordered arrangement of the channels. The MCM-48 typical structure was maintained after impregnation and calcination, though the support structure is partially collapsed or destroyed after introducing the cobalt.

Fig. 5 shows 5Co/M's structures and areas with a high density of cobalt crystallites and large areas with no cobalt present. The dark areas, marked with black arrows, give a smeared contrast over the channels, which correspond to cobalt oxide particles on the external surface. Figs. 5–7 show that cobalt oxide particles in Co/MCM-48 are present in clusters. It can be more easily found that cobalt oxide clusters concentrated more towards the external surface of the catalyst granules especially for higher Co loadings.

The cobalt crystallite size distributions obtained for the catalysts are shown in Fig. 8. The average crystallite size obtained from the above particle size distributions calculated are given in Table 2. Many of cobalt oxide particles (Fig. 8) have a diameter below 2.6 nm, which do not exceed the average pore diame-

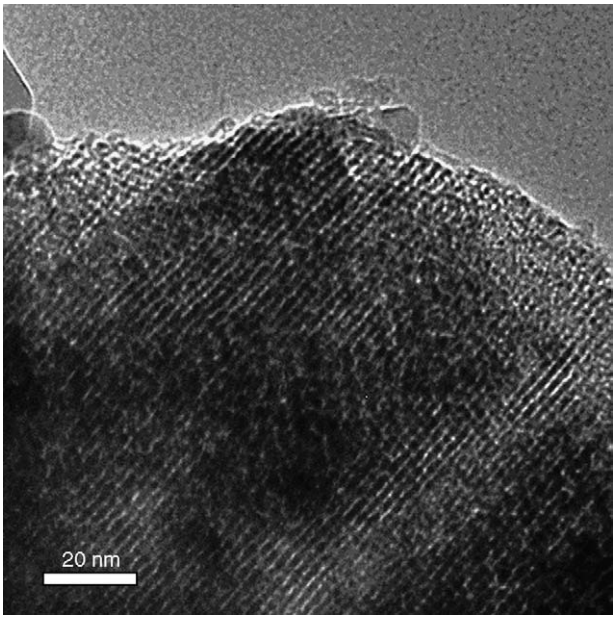

Fig. 6. TEM micrographs of 10Co/MCM-48.

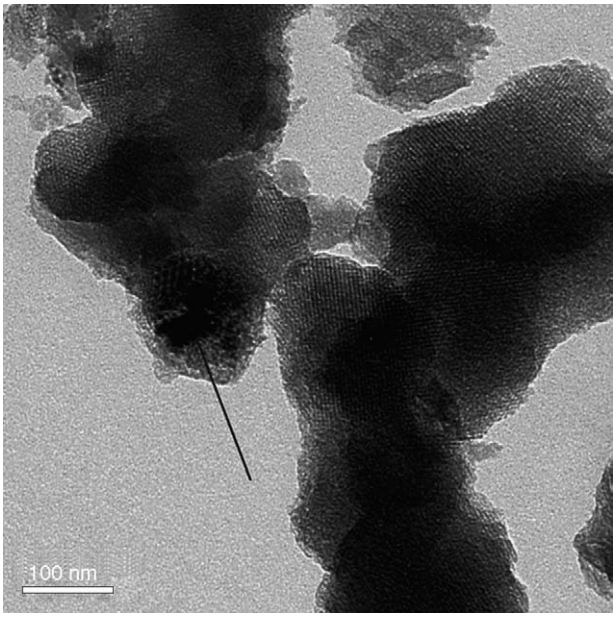

Fig. 5. TEM micrographs of 5Co/M.

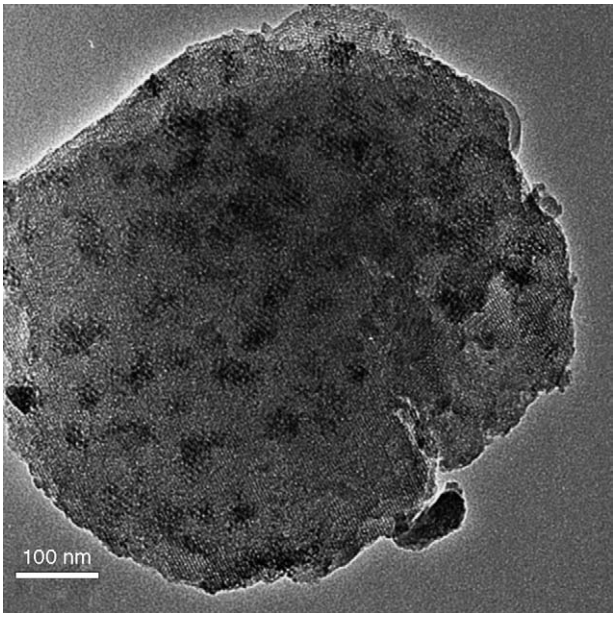

Fig. 7. TEM micrographs of 15Co/MCM-48.

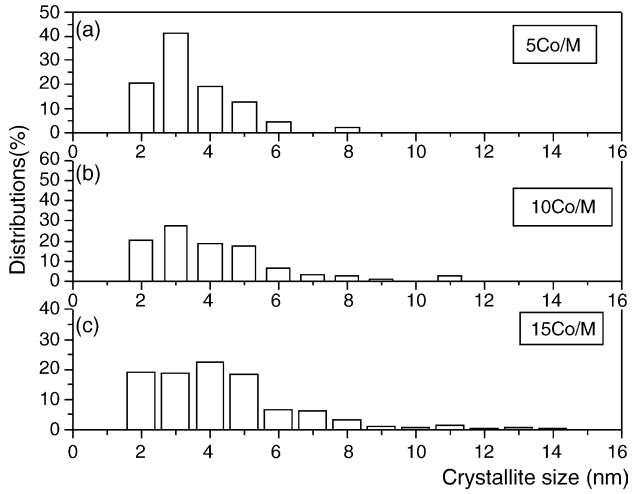

Fig. 8. Cobalt crystallites size distributions as determined by TEM.

ter of the support. It suggests that small Co crystallites were formed and stabilized in the mesoporous silica channels. The crystallites which exceed 2.6 nm were situated on the external silica grain surface near the mesopores entries resulting from the uncontrolled metal particle growth.

A pronounced maximum for particles of 3 nm diameter, representing about 40% of the total cobalt oxide particles, is found on 5Co/M (Fig. 8a). Significant differences in crystallite-size distribution are evident for three catalysts with higher cobalt content having larger Co_3O_4 distribution. The catalysts with higher cobalt loadings have bigger particles. The Co_3O_4 crystallites size of 5Co/M, 10Co/M and 15Co/M below 5 nm is about 92, 83 and 79%, respectively. Small Co metal crystallites below 5 nm appear to reoxidize and deactivate rapidly in presence of water and other reaction products at typical FTS conditions [3]. Co/MCM-48 (Fig. 4) shows a broad reduction feature in the range of 500–800 °C that could be attributed to the reduction of the smaller cobalt particles (probably those with less than 5 nm in diameter) detected by TEM. The very small cobalt oxide particles confined inside the mesoporous channels would favor the CoO–support interaction leading to the formation of hardly reducible cobalt species. Comparing the extent of reduction listed in Table 2, the three distribution values represent the crystallites which were difficult to reduce.

As seen in Table 2, XRD crystallite diameters are about 0.7–1.2 times larger than the corresponding TEM values. Usually, larger values have been reported for average particle sizes estimated from XRD as compared to other techniques and these discrepancies have been explained by considering the limitations and approximations of using XRD line broadening, which generally tend to overstate the actual particle sizes [39,40].

3.5. Fischer–Tropsch synthesis

3.5.1. Activity of Co/MCM-48 catalysts

CO conversion and the selectivity (a carbon basis) to the different FTS products are presented in Table 3. The CO conversion

Table 3
Catalytic results for the FTS on Co/MCM-48 catalysts

Catalyst	X_{CO}%[a]	S_{CO_2}%[b]	Hydrocarbon selectivity (C mol%)				
			C1	C2	C3	C4	C5+
5Co/M	1.5	3.96	23.84	3.68	4.72	3.92	59.88
10Co/M	27.1	1.36	18.82	1.14	2.54	1.9	74.23
15Co/M	25.8	1.44	17.79	1.13	2.79	2.07	74.78

The catalysts were reduced in a flow of H_2 at 723 K for 12 h before FTS. Reaction conditions: $H_2/CO = 2$, space velocity of syngas 2 S L g^{-1} h^{-1} (273 K, 0.1 MPa), temperature 503 K, pressure 10 bar.
[a] CO conversion.
[b] CO_2 selectivity.

was only 1.56% on the 5Co/M catalyst, which was almost inactive. On the other hand, taking into account experimental error, the 10Co/M and 15Co/M were quite active and no significant difference in CO conversion and C5+ selectivity.

Such a low activity on 5Co/M can be related to the low reducibility of cobalt species in the catalyst, probably in the form of cobalt silicates as discussed before. In principle, the activity of reduced Co catalysts should be proportional to the concentration of surface metal Co sites. When Co loading was low, increasing Co loading can increase the surface Co^0 sites density rapidly. At higher loading, the number of clusters increases. Also, since initially increasing the loading assists in breaking the cobalt oxide–support interaction, this allows the clusters to be more easily reduced. The true metal dispersion decreased with increasing Co loading. When Co loading reaches to 10 wt.%, increasing Co loading does not increase the surface Co^0 sites density further. As evidenced by O_2 titration, the reducibility of 10Co/M and 15Co/M are very similar (i.e., 20.4 and 21.3%, respectively). So, 10Co/M and 15Co/M showed the similar CO conversion in FTS.

3.5.2. Product selectivity

As observed in Table 3, the mesoporous 5Co/M catalyst gives the highest methane selectivity and the lowest C5+ selectivity. Increasing Co loading leads to higher C5+ selectivity. For 10Co/M and 15Co/M catalysts, selectivity to lower hydrocarbons (C1–C4) or long hydrocarbons (C5+) was similar, irrespective of the content of cobalt.

The high methane selectivity was usually reported for catalysts having high metal dispersion and low Co reducibility [7,28]. This resulted in the presence of unreduced cobalt oxides which can catalyze the WGS reaction; resulting in an increasing in H_2/CO ratio on the catalyst surface. It is known however, that an increase in effective H_2/CO ratio usually leads to both an increase in methane selectivity and to higher chain termination probability and to lower coefficient of chain propagation [23,41].

As seen in Table 3, both 10Co/M and 15Co/M present higher C5+ selectivity than 5Co/M. It is also considered that the presence of larger cobalt particles leads to higher selectivity to heavier hydrocarbons [7,15]. Also from Fig. 9, a decrease of the ratio of olefin to paraffin is showed with increasing chain length, mainly owed to the decrease of olefin content. The decrease of

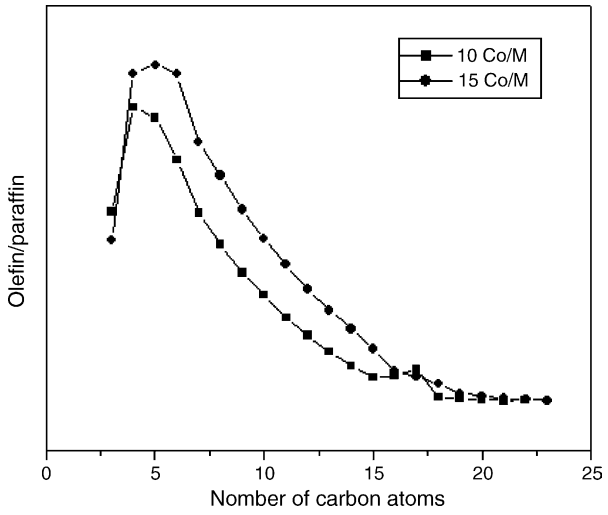

Fig. 9. Influence of Co loading on the olefin to paraffin ratio in product of catalysts. (There had no products gathered for low CO conversion of 5Co/M.)

olefin content with chain length could be caused by the decrease in the diffusivities of longer chain hydrocarbons. The increase in their residence time in the catalyst pores [3], may be caused by α-olefin readsorption [42], or the higher solubility of the higher α-olefin in the liquid phase [5], leading to their increased conversion to paraffin. So, in this study, the higher C5+ selectivity observed over 10Co/M and 15Co/M can be attributed to the following two reasons: (i) the presence of larger cobalt particles and (ii) the readsorption of the α-olefins.

The chain growth probability during Fischer–Tropsch synthesis on supported cobalt catalysts generally increases with the size of the reduced Co particles [7,23] up to a certain particle size above which it remains constant [42]. Khodakov et al. [27] also thought that for a given catalytic support hydrocarbon selectivities are almost constant in the wide range of cobalt surface densities. In this study, the C5+ selectivities followed these results.

4. Conclusions

The reducibility and FT catalytic behavior of cobalt species supported by MCM-48 can be affected by Co loading. Lower FT activity and higher methane selectivity observed on low cobalt loading catalyst are principally attributed to the lower reducibility of small cobalt particles. With increasing Co loading the cobalt crystallite size increases and leads to higher reducibility and C5+ selectivies. But when Co loading exceed 10 wt.%, the CO conversion and hydrocarbons selectivies seemed to affected slightly by Co loading. The extent of overall reduction may thus be one of the key factors for determining not only CO conversion but chain growth probability.

Acknowledgments

The work was supported by the National Natural Science Foundation of China (20473114, 20590360), Talented Young Scientist Foundation of Hubei (2003ABB013), Excellent Young Teachers Program of Ministry of Education of China, the State Ethnic Affairs Commission, PR China, and Returnee Startup Scientific Research Foundation of Ministry of Education of China.

References

[1] C. Knottenbelt, Catal. Today 71 (2002) 437.
[2] H. Schulz, Appl. Catal. A 186 (1999) 3.
[3] E. Iglesia, Appl. Catal. A 161 (1997) 59.
[4] P.J. van Berge, R.C. Everson, Stud. Surf. Sci. Catal. 107 (1997) 207.
[5] G.P. van der Laan, A.A.C.M. Beenackers, Catal. Rev. Sci. Eng. 41 (1999) 255.
[6] R. Zennaro, M. Tagliabue, C.H. Bartholomew, Catal. Today 58 (2000) 309.
[7] R.C. Reuel, C.H. Bartholomew, J. Catal. 85 (1984) 63.
[8] S. Sun, N. Tsubaki, K. Fujimoto, Appl. Catal. A 202 (2000) 121.
[9] L.B. Backman, A. Rautiainen, A.O.I. Krause, M. Lindblad, Catal. Today 43 (1998) 11.
[10] S. Bessell, Appl. Catal. A 126 (1995) 235.
[11] S. Bessell, Appl. Catal. A 96 (1993) 253.
[12] C.T. Kresge, M.E. Leonowicz, W.J. Roth, J.C. Vartuli, J.S. Beck, Nature 359 (1992) 710.
[13] S. Inagaki, Y. Fukushima, K. Kuroda, J. Chem. Soc., Chem. Commun. (1993) 680.
[14] E. Zhao, J. Feng, Q. Huo, N. Melosh, G.H. Fredrickson, B.F. Chmelka, G.D. Stucky, Science 279 (1998) 548.
[15] H.H. Nijs, P.A. Jacobs, J. Catal. 65 (1980) 328.
[16] A. Corma, Chem. Rev. 97 (1997) 2373.
[17] J. Panpranot, J.G. Goodwin Jr., A. Sayari, Catal. Today 77 (2002) 269.
[18] D. Yin, W. Li, W. Yang, H. Xiang, Y. Sun, B. Zhong, S. Peng, Microporous Mesoporous Mater. 47 (2001) 15.
[19] Y. Wang, M. Noguchi, Y. Takahashi, Y. Ohtsuka, Catal. Today 68 (2001) 3.
[20] A.Y. Khodakov, A. Griboval-Constant, R. Bechara, V.L. Zholobenko, J. Catal. 206 (2002) 230.
[21] A. Griboval-Constant, A.Y. Khodakov, R. Bechara, V.L. Zholobenko, Stud. Surf. Sci. Catal. 144 (2002) 609.
[22] A.Y. Khodakov, R. Bechara, A. Griboval-Constant, Stud. Surf. Sci. Catal. 142 (2002) 1133.
[23] A.Y. Khodakov, A. Griboval-Constant, R. Bechara, F. Villain, J. Phys. Chem. B 105 (2001) 9805.
[24] A.Y. Khodakov, J. Lynch, D. Bazin, B. Rebours, N. Zanier, B. Moisson, P. Chaumette, J. Catal. 168 (1997) 16.
[25] J. Li, G. Jacobs, Y. Zhang, T.K. Das, B.H. Davis, Appl. Catal. A 223 (2002) 195.
[26] G. Jacobs, T.K. Das, Y. Zhang, J. Li, G. Racoillet, B.H. Davis, Appl. Catal. A: Gen. 233 (2002) 263.
[27] A.Y. Khodakov, R. Bechara, A. Griboval-Constant, Appl. Catal. A: Gen. 254 (2003) 273.
[28] A. Martínez, C. López, F. Márquez, I. Díaz, J. Catal. 220 (2003) 486.
[29] S. Beck, J.C. Vartuli, W.J. Roth, M.E. Leonowicz, C.T. Kresge, K.D. Schmitt, C.T.W. Chu, D.H. Olson, E.W. Sheppard, S.B. McCullen, J.B. Higgins, J.L. Schlenker, J. Am. Chem. Soc. 114 (1992) 10834.
[30] M.W. Anderson, Zeolites 19 (1997) 220.
[31] K. Schumacher, M. Gruun, K.K. Unger, Microporous Mesoporous Mater. 27 (1999) 201.
[32] S. Wang, D. Wu, Y. Sun, B. Zhong, Acta Phys.-Chim. Sin. 17 (2001) 659.
[33] E.P. Barrett, L.G. Joyner, P.P. Halenda, J. Am. Chem. Soc. 73 (1951) 373.
[34] B.D. Cullity, Elements of X-Ray Diffraction, Addision–Wesley, London, 1978.
[35] R.D. Jones, C.H. Bartholomew, Appl. Catal. 39 (1988) 77.

[36] Y. Ohtsuka, Y. Takahashi, Catal. Today 89 (2004) 419.
[37] P. Arnoldy, J.A. Moulijn, J. Catal. 93 (1985) 38.
[38] B. Viswanathan, R. Gopalakrishnan, J. Catal. 99 (1986) 342.
[39] D.G. Castner, P.R. Watson, I.Y. Chan, J. Phys. Chem. 93 (1989) 3188.
[40] P. Ganesan, H.K. Kuo, A. Saavedra, R.J. De Angelis, J. Catal. 52 (1978) 319.
[41] A. Barbier, A. Tuel, I. Arcon, A. Kodre, G.A. Martin, J. Catal. 200 (2001) 106.
[42] E. Iglesia, S.L. Soled, R.A. Fiato, J. Catal. 137 (1992) 212.